Jurnal Jamu Indonesia (2026) 11(5): 439–448
https://jamu-journal.ipb.ac.id/index.php/JJI/index

ISSN 2407-7178
eISSN 2407-7763

Research Article
DOI: https://doi.org/10.29244/jji.v11i5.506

Molecular Docking and Molecular Dynamics of Casticin against Skin Aging Matrix Metalloproteinases

Penambatan Molekuler dan Dinamika Molekuler Casticin terhadap Matriks Metaloproteinase Terkait Penuaan Kulit

Putu G. M. W. Mahayasih[1,2*], Fadlina C. Saputri[2,3], Febrina A. Saputri[2,4], Yonatan Eden[5], Delriza S. Azahra[5], Ladisa V. Belladona[5], Sri Luliana[1,2,6], Abdul Mun'im[2,7*]

[1]*Graduate Program of Pharmaceutical Sciences, Faculty of Pharmacy, Universitas Indonesia, Depok 16424, West Java, Indonesia*
[2]*National Metabolomics Collaborative Research Center, Faculty of Pharmacy, Universitas Indonesia, Depok 16424, West Java, Indonesia*
[3]*Laboratory of Pharmacology and Toxicology, Faculty of Pharmacy, Universitas Indonesia, Depok 16424, West Java, Indonesia*
[4]*Laboratory of Pharmaceutical-Medicinal Chemistry and Bioanalysis, Faculty of Pharmacy, Universitas Indonesia, Depok 16424, West Java, Indonesia*
[5]*Department of Pharmacy, Faculty of Health Sciences, Universitas Esa Unggul, Jakarta 11510, DKI Jakarta, Indonesia*
[6]*Department of Pharmaceutical Chemistry, Faculty of Pharmacy, Universitas Tanjungpura, Pontianak 78124, West Kalimantan, Indonesia*
[7]*Cluster of Herbal Drug Discovery & Development, Faculty of Pharmacy, Universitas Indonesia, Depok 16424, West Java, Indonesia*

ARTICLE INFO

Article history
Received on: 2026-04-07
Revised on: 2026-09-03
Accepted on: 2026-09-04

Keywords:
Casticin;
matrix metalloproteinases;
molecular docking;
molecular dynamics;
skin aging

Kata kunci:
Casticin;
matriks metaloproteinase;
penambatan molekuler;
dinamika molekuler;
penuaan kulit

ABSTRACT

Skin aging involves extracellular-matrix degradation mediated in part by matrix metalloproteinases (MMP-1, MMP-9, and MMP-12). This study evaluated casticin interactions with these enzymes using AutoDock Vina docking followed by 100-ns molecular dynamics simulations. Casticin produced docking scores of -8.4, -7.7, and -9.0 kcal/mol for MMP-1, MMP-9, and MMP-12, respectively. For MMP-12, its score was slightly more negative than that of EGCG (-8.7 kcal/mol). During MD, casticin maintained relatively low ligand-conformation RMSD while showing appreciable ligand-movement RMSD, indicating preservation of internal geometry despite positional rearrangement. Protein compactness remained broadly preserved in the ligand-bound trajectories. These findings support further biochemical evaluation of casticin against skin-aging-related MMPs.

ABSTRAK

Penuaan kulit melibatkan degradasi matriks ekstraseluler yang sebagian dimediasi oleh matrix metalloproteinases (MMP-1, MMP-9, dan MMP-12). Penelitian ini mengevaluasi interaksi casticin dengan ketiga enzim tersebut menggunakan molecular docking dengan AutoDock Vina yang dilanjutkan dengan simulasi molecular dynamics selama 100 ns. Casticin menghasilkan docking score masing-masing sebesar -8,4, -7,7, dan -9,0 kcal/mol terhadap MMP-1, MMP-9, dan MMP-12. Pada MMP-12, docking score casticin sedikit lebih negatif dibandingkan EGCG (-8,7 kcal/mol). Selama simulasi MD, casticin menunjukkan ligand-conformation RMSD yang relatif rendah disertai ligand-movement RMSD yang cukup besar, menunjukkan terjaganya geometri internal meskipun terjadi perubahan posisi ligan. Kekompakan struktur protein secara umum tetap terjaga pada trajektori kompleks protein–ligan. Temuan ini mendukung evaluasi biokimia lebih lanjut terhadap casticin pada MMP yang berkaitan dengan penuaan kulit.

**Corresponding authors:*
Putu G. M. W. Mahayasih (putu.gitamaya@esaunggul.ac.id); Abdul Mun'im (munim@farmasi.ui.ac.id)

Citation: Mahayasih, P. G. M. W., Saputri, F. C., Saputri, F. A., Eden, Y., Azahra, D. S., Belladona, L. V., Luliana, S., & Mun'im, A. (2026). Molecular Docking and Molecular Dynamics of Casticin against Skin Aging Matrix Metalloproteinases. *Jurnal Jamu Indonesia*, *11*(5), 439–448. https://doi.org/10.29244/jji.v11i5.506

© 2026 Authors. This is an open-access article distributed under the terms of the Creative Commons Attribution-NonCommercial-ShareAlike 4.0 International License (http://creativecommons.org/licenses/by-nc-sa/4.0/)

1. INTRODUCTION

Skin aging is a multifactorial biological process driven by intrinsic and extrinsic factors, particularly ultraviolet (UV) radiation. At the molecular level, one of the major events in skin aging is the progressive degradation of the extracellular matrix (ECM), which contributes to loss of elasticity, wrinkle formation, dermal thinning, and structural deterioration of the skin (Păcularu-Burada et al., 2024). The ECM is mainly composed of structural proteins such as collagen and elastin, whose integrity is essential for maintaining dermal strength and elasticity. Excessive degradation of these components is largely mediated by matrix metalloproteinases (MMPs), a family of zinc-dependent endopeptidases involved in ECM remodeling and degradation (Feng et al., 2024).

The expression of MMPs is commonly increased under UV-induced oxidative stress and inflammatory conditions through the activation of signaling pathways involving transcription factors such as activator protein-1 (AP-1) and nuclear factor-kappa B (NF-κB), leading to collagen fragmentation, elastin degradation, impaired dermal repair, and progressive weakening of the skin structure (Islam et al., 2024). Among the MMP family, MMP-1, MMP-9, and MMP-12 are particularly relevant to skin-aging-related ECM degradation because they act on complementary components of the dermal matrix. MMP-1 initiates the cleavage of fibrillar collagen, MMP-9 participates in collagen degradation and basement membrane remodeling, whereas MMP-12 is associated with elastin degradation and broader ECM remodeling. These three enzymes were therefore selected to represent key molecular targets involved in collagen degradation, matrix remodeling, and elastin breakdown during intrinsic aging and photoaging (Dorjay Tamang et al., 2025; Gimeno et al., 2020).

Natural products, particularly flavonoid-rich medicinal plants, have attracted attention as potential sources of bioactive compounds for skin aging research because of their antioxidant, anti-inflammatory, and enzyme-interaction properties (Păcularu-Burada et al., 2024). *Vitex trifolia* L., locally known as legundi, is a medicinal plant traditionally used in Asian ethnomedicine and has been increasingly investigated for its skin-protective potential. Recent studies reported that *V. trifolia* leaf extract exhibits antioxidant activity, collagenase and elastase inhibitory effects, cytoprotective activity against UVB-induced damage in HaCaT keratinocytes, and downregulation of UVB-induced MMP-1 and MMP-9 expression, supporting its relevance as a potential anti-photoaging natural source (Mahayasih et al., 2026). From a phytochemical perspective, casticin is a polymethoxylated flavonoid associated with *Vitex* species that has been studied mainly for its anti-inflammatory and antineoplastic properties (Abbas et al., 2025; Carbone et al., 2023; Ramchandani et al., 2020), and it has been reported as a major metabolite in *V. trifolia* leaf extract. LC–HRMS profiling of an ethanolic *V. trifolia* extract identified casticin as the predominant metabolite with the highest AUC among the detected compounds, and other metabolite profiling studies have also reported casticin across different *V. trifolia* extracts (Mahayasih et al., 2026; Masruri et al., 2025). These findings provide a strong rationale for selecting casticin as a marker compound and representative bioactive constituent of *V. trifolia* in the present computational study.

Although our previous study demonstrated the broader anti-photoaging potential of *V. trifolia* through integrated *in vitro* and *in silico* approaches, the molecular behavior of casticin toward multiple matrix metalloproteinases has not been systematically characterized within a dedicated docking and molecular dynamics framework. This study therefore aimed to characterize the predicted interactions of casticin with MMP-1, MMP-9, and MMP-12 using an independent AutoDock Vina-based docking protocol followed by 100-ns molecular dynamics simulations with the AMBER14 force field. No prepared protein structures, docking poses, molecular-dynamics trajectories, or trajectory-derived analyses from the previous study were reused here. The design allows a focused comparison of casticin across three MMP targets involved in collagen degradation, matrix remodeling, and elastin breakdown, together with trajectory-based information on its conformational and positional behavior under the simulated conditions. The study thus provides complementary computational evidence beyond the broader phytochemical screening reported previously and supports further experimental evaluation of casticin (Mechqoq et al., 2022; Zheng et al., 2024).

2. METHODS

2.1. Protein and Ligand Preparation

The protein structures of matrix metalloproteinase-1 (MMP-1; PDB ID: 966C), MMP-9 (PDB ID: 6ESM), and MMP-12 (PDB ID: 1JIZ) were obtained from the Protein Data Bank. Chain A was selected for all three receptors, with crystallographic resolutions of 1.90 Å, 1.10 Å, and 2.60 Å for MMP-1, MMP-9, and MMP-12, respectively. Receptor preparation was performed using PyMOL 3.0.3 (Schrödinger, LLC, New York, NY, USA) and AutoDockTools 1.5.7 (Scripps Research, La Jolla, CA, USA). The crystallographic native ligands were separated and retained for redocking validation. Catalytic Zn^{2+} and structural Ca^{2+} ions were retained in their crystallographic positions, whereas non-essential heteroatoms and all crystallographic water molecules were removed. Residues surrounding the catalytic Zn^{2+} site were inspected during receptor preparation, and distances between catalytic Zn^{2+} and the coordinating atoms of the crystallographic native ligands were examined as a structural check before docking. No catalytic or metal-associated crystallographic water was intentionally retained.

In the final receptor PDBQT files, the retained Zn atoms carried a partial charge of 0.000. No zinc-specific pseudoatom model, specialized zinc-coordination potential, or metal–ligand distance restraint was introduced. Zn-mediated interactions were therefore interpreted within the limitations of the standard AutoDock Vina scoring scheme.

Casticin (PubChem CID 5315263), epigallocatechin gallate (EGCG; CID 65064), and resveratrol (CID 445154) were prepared as ligands. Structures were drawn and verified in MarvinSketch 23.12 (ChemAxon, Budapest, Hungary), and protonation states were assigned at pH 7.4. No tautomer enumeration was performed. A single three-dimensional conformer was generated and geometry-optimized using the MMFF94 force field, with the optimization level set to Normal and energies expressed in kcal/mol. The optimized structures were exported in PDB format and converted to PDBQT using AutoDockTools 1.5.7, where Gasteiger charges were assigned. EGCG was used as the comparative natural-product ligand for MMP-1 and MMP-12, whereas resveratrol was used for MMP-9, based on experimental literature reporting MMP-related activity for the corresponding target.

2.2. Molecular Docking Validation and Analysis

Docking protocol validation was performed by redocking each crystallographic ligand into the corresponding binding site. Validation was considered acceptable when the RMSD between the redocked and crystallographic poses was <2.0 Å. The native ligands were RS2 for MMP-1 (966C), B9Z for MMP-9 (6ESM), and CGS for MMP-12 (1JIZ). Grid-center coordinates and box dimensions are reported in Å in **Table 1** (Bell & Zhang, 2019; Nutho & Tungmunnithum, 2023).

Docking grids were centered on the crystallographic ligand-binding sites using the coordinates and dimensions listed in **Table 1**. Exhaustiveness was set to 32, and up to nine poses were generated per ligand. The top-ranked pose was selected on the basis of the most negative AutoDock Vina docking score and was inspected in Discovery Studio Visualizer v25.1.0.24284 (BIOVIA, Dassault Systèmes, San Diego, CA, USA). Docking output was expressed as AutoDock Vina docking scores (kcal/mol) and used to compare the predicted binding poses of the tested ligands within the selected binding sites. Scores were interpreted comparatively under identical docking conditions (Nutho & Tungmunnithum, 2023).

EGCG was selected as the comparative ligand for MMP-1 on the basis of experimental evidence that it suppresses MMP-1 expression and secretion in human dermal fibroblasts and affects MMP-1-related collagenolytic activity (Bae et al., 2008). For MMP-12, EGCG was chosen because green-tea catechins, including EGCG, have been reported to inhibit MMP-12 activity (Demeule et al., 2000). Resveratrol was selected for MMP-9 because it reduces MMP-9 expression in UVB-induced photoaging models (Cui et al., 2022) and suppresses MMP-9 expression and secretion in other cell models (Zhang et al., 2019). These compounds were therefore used as comparative natural-product ligands in the present docking analysis.

Table 1. Validation of the molecular docking protocol by redocking crystallographic ligands. RMSD, root-mean-square deviation.

PDB ID	Native ligand	Grid center (x, y, z; Å)	Grid box size (x, y, z; Å)	RMSD (Å)	Validation status
966C	RS2	9.166, -10.353, 38.398	20, 22, 22	1.119	Valid
6ESM	B9Z	0.794, 50.361, 19.921	20, 22, 22	1.387	Valid
1JIZ	CGS	1.302, 4.330, 70.394	20, 30, 22	1.361	Valid

2.3. Molecular Dynamics Simulation

Protein–ligand complexes obtained from docking were merged in PyMOL 3.0.3 and used as starting structures for MD simulations in YASARA Dynamics 25.1.15 (YASARA Biosciences GmbH, Vienna, Austria) with the AMBER14 force field. The standard YASARA md_run workflow was used with study-specific settings of pH 7.4, 310 K, 100-ns duration, and a 100-ps snapshot interval. Each solute was placed in a cubic periodic simulation cell extending 10 Å beyond the solute on each side and solvated in an explicit aqueous environment. Na^+ and Cl^- were added at 0.9% mass fraction (w/w). The non-bonded cutoff was 8 Å, and long-range Coulomb interactions were treated using particle-mesh Ewald electrostatics. Catalytic Zn^{2+} and structural Ca^{2+} ions present in the prepared starting structures were retained. Neither the simulation macro nor the YASARA console output specified an explicit water model (e.g., TIP3P, TIP4P, or SPC), so no water-model name is assigned here (Irsal et al., 2024; Land & Humble, 2018).

Temperature was controlled at 310 K using the YASARA temperature-control procedure, whereas pressure and density control used SolventProbe mode with water density set to 0.997 g/mL. Energy minimization was performed before production dynamics, and the applied macro did not define a separate equilibration stage between minimization and production. The normal-speed setting was used, corresponding to a multiple timestep with a total timestep of 2.5 fs; bonds and angles were not constrained in this mode. No positional or distance restraints were applied to the protein, catalytic Zn^{2+}, Ca^{2+}, or metal-coordinating residues, and no manual metal-specific parameterization was introduced beyond the standard YASARA/AMBER14 workflow. Trajectory snapshots were saved every 100 ps (Irsal et al., 2024; Land & Humble, 2018).

Simulation trajectories were analyzed using YASARA trajectory-analysis macros to calculate ligand-conformation RMSD, ligand-movement RMSD, residue RMSF, radius of gyration (Rg), and, where available, protein Cα and backbone RMSD. Each protein–ligand system was simulated as a single trajectory because of computational-resource limitations. All comparisons are therefore reported as descriptive observations from individual trajectories; trajectory frames were not treated as independent biological or simulation replicates, and no claim of statistically established superiority is made (Land & Humble, 2018; Astuti et al., 2024).

3. RESULTS AND DISCUSSION

3.1. Molecular Docking Analysis

Casticin returned favorable docking scores against MMP-1, MMP-9, and MMP-12, reflecting its predicted interaction within the selected binding pockets under the applied docking conditions. The corresponding docking scores and interaction profiles of casticin, EGCG, and resveratrol are presented in **Table 2** and **Figure 1**.

Casticin showed favorable docking scores across the three MMP targets, although the relative scores differed depending on the receptor. For MMP-1, casticin gave a docking score of -8.4 kcal/mol, close to that of EGCG (-8.6 kcal/mol), and its predicted pose involved several hydrogen-bonding and hydrophobic contacts within the selected binding pocket, indicating a comparable predicted binding profile for the two ligands. In MMP-9, casticin scored -7.7 kcal/mol, whereas resveratrol produced a more negative score of -8.9 kcal/mol. The predicted casticin pose formed hydrogen-bond and hydrophobic contacts with residues including TYR248, MET247, GLY186, HIS226, and VAL223. These contacts are consistent with accommodation of casticin within the selected MMP-9 binding pocket, although its docking score was less negative than that of resveratrol under the applied docking conditions.

Table 2. AutoDock Vina docking scores and residue-level interactions of casticin with MMP-1, MMP-9, and MMP-12 in comparison with the selected comparative natural-product ligands. EGCG, epigallocatechin gallate.

Receptor	Ligand	AutoDock Vina docking score (kcal/mol)	Interaction	Amino acid residue and binding distance (Å)
MMP-1	Casticin	-8.4	Hydrogen bonding	LEU181 (2.244 Å), ALA182 (2.746 Å), TYR237 (1.847 Å), SER239 (2.358 Å), THR241 (3.683 Å), GLY179 (2.245 Å), LEU235 (2.746 Å)
			Hydrophobic	HIS218 (4.636 Å), TYR240 (5.333 Å), VAL215 (4.627 Å)
	EGCG	-8.6	Hydrogen bonding	ALA182 (2.797 Å), ASN180 (2.539 Å), ALA184 (2.143 Å), GLU219 (2.609 Å), HIS218 (3.075 Å)
			Hydrophobic	HIS218 (3.758 Å)
MMP-9	Casticin	-7.7	Hydrogen bonding	LEU187 (2.832 Å), TYR248 (2.409 Å), MET247 (2.131 Å), TYR245 (2.446 Å), GLY186 (2.430 Å), LEU243 (2.942 Å)
			Hydrophobic	HIS226 (3.786 Å), VAL223 (4.909 Å), TYR248 (5.202 Å)
	Resveratrol	-8.9	Hydrogen bonding	GLN227 (2.785 Å), ARG249 (2.378 Å), ALA189 (2.644 Å), LEU243 (3.067 Å), TYR245 (2.485 Å), ALA242 (2.811 Å)
			Hydrophobic	LEU188 (4.864 Å), LEU222 (5.323 Å), VAL223 (4.761 Å), LEU243 (5.137 Å), ARG249 (5.049 Å), HIS226 (4.429 Å)
MMP-12	Casticin	-9.0	Hydrogen bonding	LEU82 (2.795 Å), PHE138 (1.961 Å), THR140 (2.532 Å), PRO139 (3.482 Å)
			Hydrophobic	HIS119 (3.948 Å), LEU115 (4.538 Å), TYR141 (4.430 Å), LEU82 (5.106 Å)
	EGCG	-8.7	Hydrogen bonding	ALA83 (2.356 Å), GLY80 (1.934 Å), PHE138 (1.950 Å), THR140 (2.712 Å), GLU120 (2.338 Å), HIS84 (3.424 Å)
			Hydrophobic	HIS119 (3.895 Å), HIS129 (4.977 Å)
			Electrostatic	Zn^{2+} 257 (3.366 Å)

Among the three targets, casticin showed its most negative docking score against MMP-12 (-9.0 kcal/mol), compared with -8.7 kcal/mol for EGCG. The predicted pose was characterized by hydrogen bonds with LEU82, PHE138, THR140, and PRO139, together with hydrophobic contacts involving HIS119, LEU115, TYR141, and LEU82. This combination of polar and hydrophobic

interactions suggests favorable accommodation of casticin within the selected MMP-12 binding pocket. The difference from EGCG was nevertheless small, indicating broadly comparable predicted binding under the applied docking conditions. Taken as a whole, the docking results show target-dependent differences in both docking score and residue-level interaction pattern. These initial poses were then examined by molecular dynamics simulation to characterize their conformational and positional behavior over the 100-ns trajectories.

3.2. Molecular Dynamics

The dynamic behavior of the protein-ligand systems was further examined using 100-ns molecular dynamics (MD) simulations. The trajectory analysis focused on ligand-conformation RMSD, ligand-movement RMSD, protein RMSF, radius of gyration (Rg), and protein RMSD where available. Because ligand-to-Zn distance, ligand-to-active-site-center distance, and contact-occupancy analyses were not performed, the MD results were not used to establish persistent active-site binding or ligand retention.

3.2.1. Root Mean Square Deviation (RMSD)

RMSD was used to describe structural deviation during the simulations. Ligand-conformation RMSD measures changes in the ligand's internal geometry after fitting, whereas ligand-movement RMSD reflects positional displacement relative to the initial binding pose. These two measures were therefore interpreted separately. Protein Cα/backbone RMSD was additionally considered as an indicator of protein structural deviation where analysis was available (Tan et al., 2024). Ligand-conformation RMSD profiles are shown in **Figure 2**, and ligand-movement RMSD profiles in **Figure 3**.

In the MMP-1 system, casticin showed a higher mean ligand-movement RMSD than EGCG (5.188 vs. 1.911 Å), while its ligand-conformation RMSD remained low (1.136 Å). This indicates that casticin largely preserved its internal geometry despite greater displacement from the initial docking pose. The mean protein Cα/backbone RMSD values were 1.529/1.581 Å for MMP-1–casticin and 1.185/1.244 Å for MMP-1–EGCG, indicating limited overall protein deviation in both trajectories.

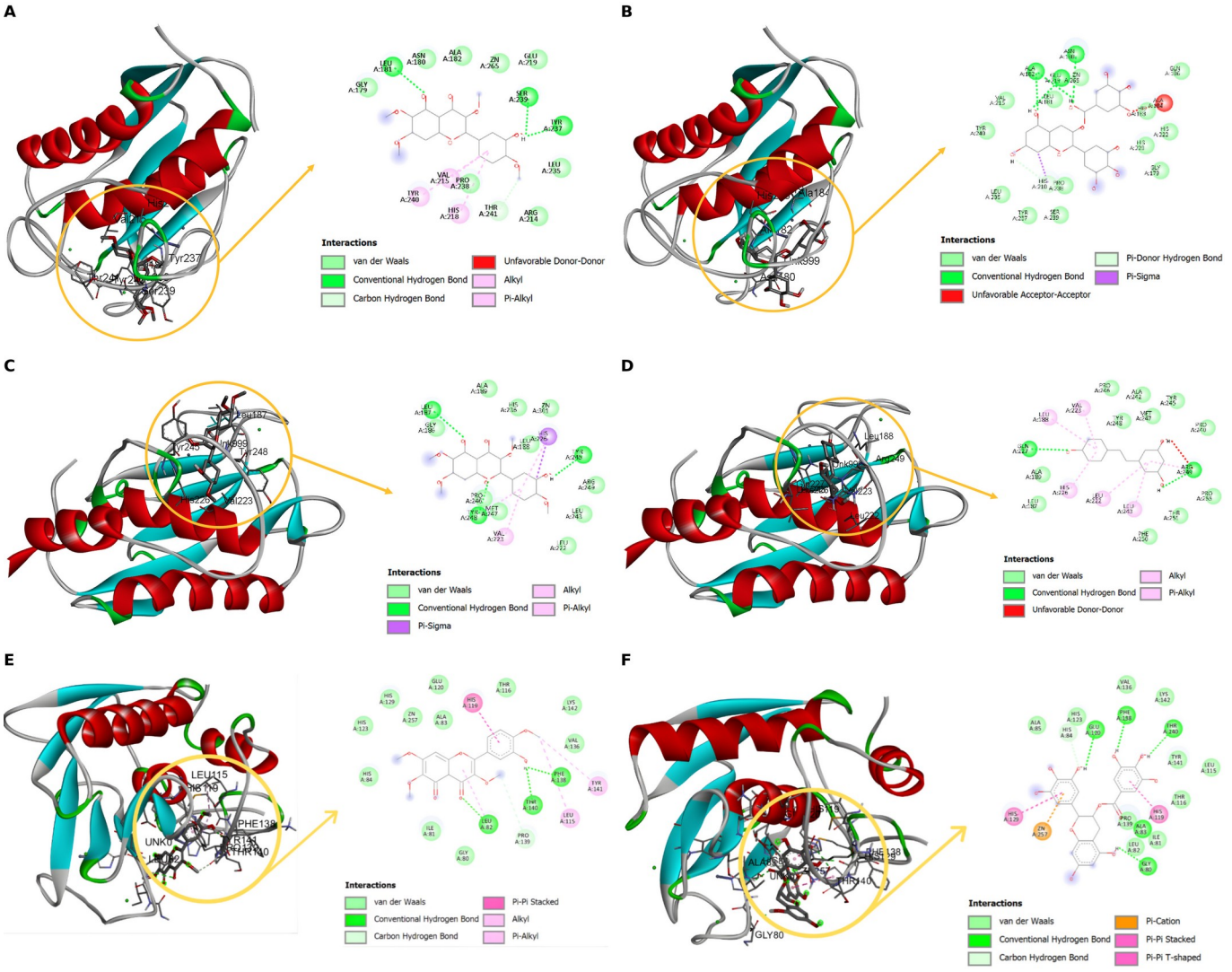

Figure 1. Predicted three-dimensional binding poses (left of each panel) and the corresponding two-dimensional interaction diagrams (right of each panel) for MMP-1 with casticin (A) and EGCG (B), MMP-9 with casticin (C) and resveratrol (D), and MMP-12 with casticin (E) and EGCG (F). EGCG, epigallocatechin gallate.

For MMP-9, casticin also showed greater ligand movement than resveratrol (4.057 vs. 1.828 Å), whereas their ligand-conformation RMSD values were comparable (1.280 vs. 1.381 Å). The mean protein Cα/backbone RMSD values were 1.618/1.764 Å for MMP-9–casticin and 1.241/1.415 Å for MMP-9–resveratrol, again showing relatively limited global structural deviation.

In MMP-12, casticin had a higher mean ligand-movement RMSD than EGCG (4.767 vs. 2.875 Å), while ligand-conformation RMSD values were similar (1.845 vs. 1.895 Å). The mean Cα/backbone RMSD values were 0.972/1.012 Å for MMP-12–casticin and 1.042/1.071 Å for MMP-12–EGCG, representing the lowest protein RMSD values among the three systems. Overall, casticin consistently maintained relatively low conformational RMSD while showing greater positional displacement, particularly in MMP-1. Protein RMSD values remained comparatively low across all three targets, indicating preservation of the global protein structure during the simulations.

Because ligand-to-Zn distance, active-site-center distance, and contact-occupancy analyses were not performed, these RMSD data do not establish continuous retention of casticin within the catalytic region throughout the 100-ns trajectories.

3.2.2. Root Mean Square Fluctuation (RMSF) at Key Residues

RMSF analysis was used to assess residue flexibility during the simulations; the resulting profiles are shown in **Figure 4**.

In the MMP-1 ligand-bound trajectories (**Figure 4A**), LEU181, ALA182, VAL215, GLU219, and TYR240 generally showed limited fluctuations. Among these residues, TYR240 displayed a higher RMSF in the casticin complex than in the EGCG complex (1.72 vs. 1.23 Å), indicating a difference in local mobility around this region. A similar pattern was observed for MMP-9 (**Figure 4B**), where VAL223, HIS226, GLN227, LEU243, and ARG249 showed low-to-moderate fluctuations, and ARG249 was more flexible in the casticin trajectory than in the resveratrol trajectory (2.59 vs. 1.37 Å). RMSF analysis is commonly used in MD studies to identify residue-specific differences in protein mobility and has also been applied to characterize dynamic behavior within MMP–ligand complexes (Mathpal et al., 2022). Because simulations of the unliganded proteins were not included, these differences are interpreted as variations between ligand-bound trajectories rather than as ligand-induced changes relative to the unliganded state.

For MMP-12 (**Figure 4C**), residues within and around the selected catalytic-region pocket, including HIS119, PHE138, PRO139, THR140, and TYR141, also fluctuated modestly in both ligand-bound systems. HIS119 and TYR141 fluctuated less in the casticin trajectory, whereas PHE138 and PRO139 showed slightly lower RMSF values in the EGCG trajectory. The absence of a uniform trend across these residues suggests that the two ligands were associated with different local mobility patterns within the MMP-12 pocket. Such residue-level variation is consistent with the dynamic nature of MMP binding regions, where local flexibility can influence ligand recognition and accommodation within the catalytic and specificity regions. Because residue-contact persistence was not evaluated, however, the RMSF profiles cannot determine whether the contacts observed in the initial docking poses were maintained throughout the simulation.

Overall, the RMSF profiles showed relatively limited residue fluctuations across the three ligand-bound MMP systems, with

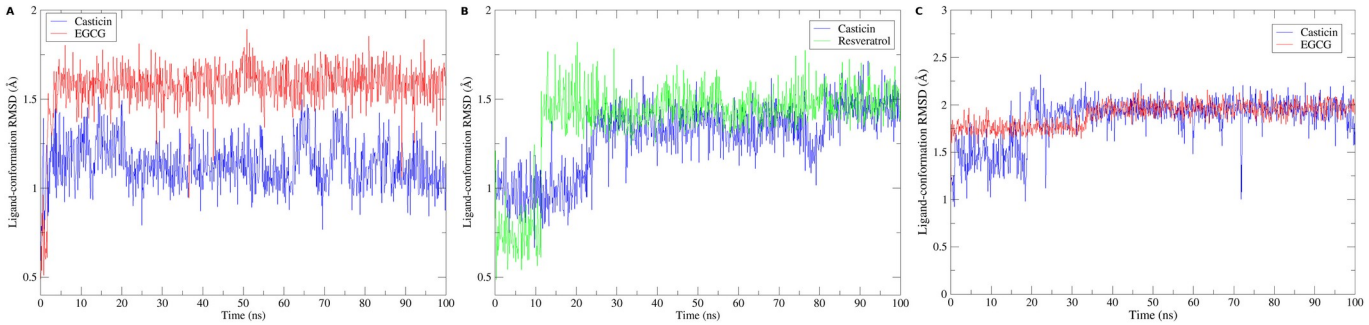

Figure 2. Ligand root-mean-square deviation (RMSD) profiles describing ligand conformational stability of casticin compared with the comparative natural-product ligands EGCG or resveratrol in complex with (A) MMP-1, (B) MMP-9, and (C) MMP-12. EGCG, epigallocatechin gallate.

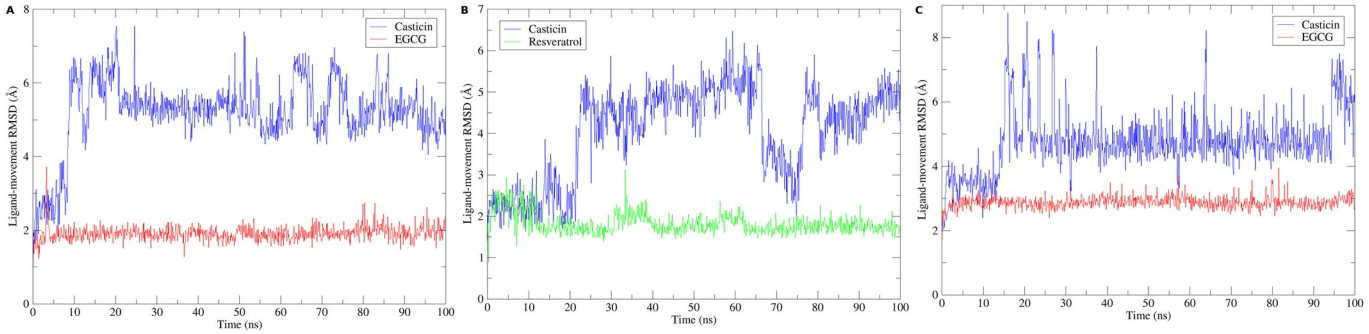

Figure 3. Root-mean-square deviation (RMSD) profiles describing ligand positional fluctuation (ligand movement) of casticin compared with the comparative natural-product ligands EGCG or resveratrol in complex with (A) MMP-1, (B) MMP-9, and (C) MMP-12.

more pronounced differences at selected residues such as TYR240 in MMP-1 and ARG249 in MMP-9. These differences reflect local variations in residue mobility and are best considered together with the RMSD and Rg results when describing the dynamic behavior of the complexes. RMSF alone does not establish persistent ligand binding or stabilization relative to an unliganded protein. This distinction is particularly important for metalloproteinases, where the catalytic Zn^{2+} environment and its surrounding residues form a dynamic coordination network that cannot be assessed solely from atomic fluctuation values. Studies of MMP catalytic zinc sites have shown that metal coordination, surrounding water molecules, and local protein dynamics are closely interconnected (Chakrabarti et al., 2017). Accordingly, low fluctuation of Zn^{2+} or nearby residues in the present trajectories should be interpreted as limited positional variation during the simulation, without implying persistent ligand–Zn coordination.

3.2.3. Radius of Gyration (Rg)

The radius of gyration (Rg) was used to evaluate changes in the overall compactness of the protein structures during the simulations (Maghfira et al., 2025; Misra & Yadav, 2022). Relatively consistent Rg values throughout a trajectory indicate that the global compactness of the protein is largely maintained, whereas larger changes may reflect alterations in its overall structural organization (Irsal et al., 2024). The Rg profiles are presented in **Figure 5**.

The Rg profiles remained relatively consistent across all ligand-bound systems. Mean Rg values were 15.185 and 15.065 Å for MMP-1 complexed with casticin and EGCG, respectively; 14.971 and 14.812 Å for MMP-9 with casticin and resveratrol; and 14.992 and 15.042 Å for MMP-12 with casticin and EGCG. The relatively narrow differences between the paired trajectories indicate that the overall protein compactness was maintained during the 100-ns simulations. MMP-12 showed particularly similar mean Rg values for the two ligand-bound systems, consistent with the low protein Cα and backbone RMSD observed for this target. Overall, the Rg results complement the protein RMSD findings by showing limited changes in global protein dimensions throughout the simulations. However, Rg describes protein compactness and does not provide information on ligand retention within the binding pocket.

Taken together, the docking and MD results show that casticin displayed target-dependent dynamic behavior across the three MMP systems. During the simulations, casticin generally maintained its internal conformation while showing appreciable positional movement from the initial docking pose. The Rg profiles indicated preservation of global protein compactness, whereas RMSF reflected residue-level mobility within the ligand-bound trajectories. Because ligand-to-Zn distance, ligand-to-active-site-center distance, hydrogen-bond occupancy, and residue-contact persistence were not evaluated, the docking poses are considered predicted starting interactions and were not used to infer persistent active-site binding throughout the 100-ns simulations.

The docking poses placed casticin within the selected catalytic-domain binding regions and identified interactions with residues surrounding the corresponding pockets. However, the persistence of these contacts during MD was not assessed. Therefore, differences among the three MMP systems were interpreted primarily from the observed RMSD, RMSF, and Rg profiles, without attributing them to sustained interactions with the catalytic Zn^{2+} region or the S1′ specificity pocket. Further

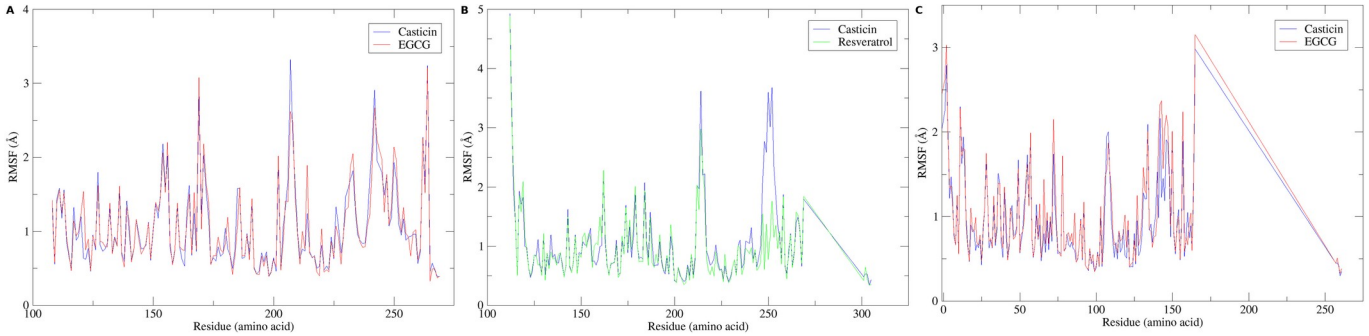

Figure 4. Root-mean-square fluctuation (RMSF) profiles of protein residues in casticin complexes compared with the comparative natural-product ligands EGCG or resveratrol during 100-ns molecular dynamics simulations of (A) MMP-1, (B) MMP-9, and (C) MMP-12.

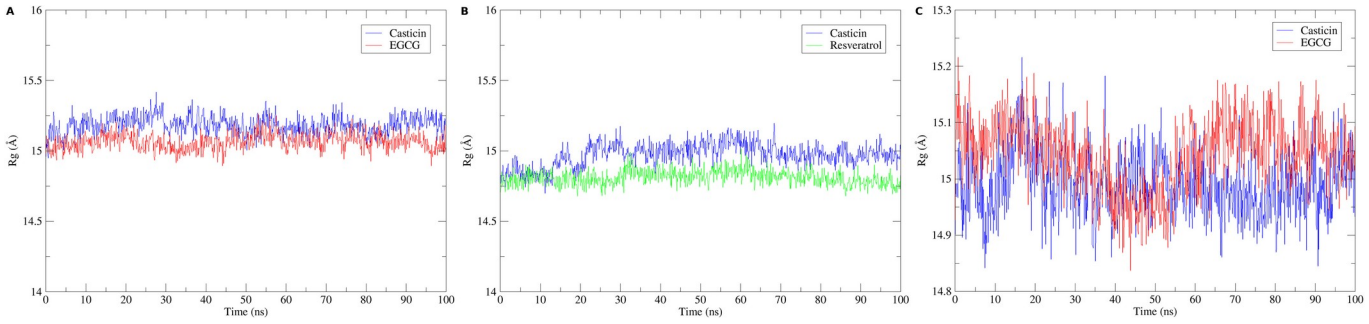

Figure 5. Radius of gyration (Rg) profiles describing protein compactness for casticin complexes relative to the comparative natural-product ligands EGCG or resveratrol during 100-ns molecular dynamics simulations of (A) MMP-1, (B) MMP-9, and (C) MMP-12.

trajectory-based distance and contact analyses would be required to examine these interactions in greater detail.

This study has several limitations. First, the findings are based entirely on computational analyses and require experimental confirmation of MMP inhibition. Second, conventional AutoDock Vina scoring was used without a zinc-specific docking potential, and all crystallographic waters, including metal-associated waters, were removed during receptor preparation; these choices limit interpretation of metal-coordination and water-mediated interactions at the catalytic site. Third, each protein–ligand complex was represented by a single 100-ns trajectory, so run-to-run variability was not assessed, and multiple independent trajectories are generally recommended for more reliable characterization of protein–ligand interactions (Wu et al., 2024). Simulations of the unliganded proteins were also not performed, which limits conclusions regarding ligand-associated changes in protein flexibility. Finally, ligand-to-Zn distance, active-site-center distance, hydrogen-bond occupancy, and residue-contact persistence were not analyzed, preventing detailed assessment of long-term ligand positioning within the catalytic region. Further biochemical and cell-based studies, together with more detailed trajectory analyses, are needed to validate and extend these findings.

4. CONCLUSION

This study provides a descriptive computational characterization of casticin in MMP-1, MMP-9, and MMP-12 systems. Casticin generated favorable AutoDock Vina docking scores and maintained relatively low ligand-conformation RMSD during 100-ns MD, while ligand-movement RMSD showed appreciable positional rearrangement. The results support casticin as a candidate for further investigation but do not establish superior affinity, persistent active-site retention, MMP inhibition, or anti-aging efficacy. Additional trajectory-based distance/contact analyses, independent simulation replicates, biochemical enzyme assays, and cell-based validation would be required to address these questions directly.

AUTHOR CONTRIBUTIONS

Conceptualization, P.G.M.W.M. and A.M.; methodology, P.G.M.W.M., Y.E., D.S.A., L.V.B.; software, P.G.M.W.M. and A.M.; validation, D.S.A., L.V.B., S.L.; formal analysis, F.A.S. and Y.E.; investigation, F.C.S. and Y.E.; data curation, A.M., F.C.S., and F.A.S.; writing—original draft preparation, P.G.M.W.M., D.S.A., L.V.B., A.M.; writing—review and editing, P.G.M.W.M., A.M., F.C.S., S.L., and F.A.S.; visualization, D.S.A. and L.V.B.; supervision, A.M., P.G.M.W.M., Y.E.; project administration, Y.E.; funding acquisition, A.M., P.G.M.W.M. All authors have read and agreed to the published version of the manuscript.

INSTITUTIONAL REVIEW BOARD STATEMENT

Not applicable. This study did not involve humans or animals.

INFORMED CONSENT STATEMENT

Not applicable.

DATA AVAILABILITY STATEMENT

The docking input files, molecular dynamics input files, processed trajectory data, and analysis files are available from the corresponding author upon reasonable request.

FUNDING

This research was funded by the Indonesian Endowment Fund for Education (LPDP), grant number LOG-776/LPDP.3/2024.

ACKNOWLEDGMENT

The authors thank the affiliated institutions for their assistance during the preparation and analysis of this study.

CONFLICTS OF INTEREST

The authors declare no conflict of interest.

ROLE OF FUNDERS

The funders had no role in the design of the study; in the collection, analyses, or interpretation of data; in the writing of the manuscript, or in the decision to publish the results.

DECLARATION OF GENERATIVE ARTIFICIAL INTELLIGENCE (AI) USE

During the preparation of this manuscript, the authors used ChatGPT (OpenAI) to assist in improving the clarity, structure, or readability of the text. After using this tool, the authors thoroughly reviewed, edited, and verified the entire content to ensure it accurately represents their own ideas and interpretations. The authors take full responsibility for the integrity and originality of the published work.

REFERENCES

Abbas, S., Shahbaz, M., Ali, A., Irshad, S., Ahmad, S., Seelan, J. S. S., Wiart, C., Palasuberniam, P., & Mustaffa, N. (2025). Casticin: A natural flavonoid with promising pharmacological and biological activities. *Fitoterapia*, *185*, 106746. https://doi.org/10.1016/j.fitote.2025.106746

Astuti, P. D. Y., Fadilah, F., Promsai, S., & Bahtiar, A. (2024). Integrating molecular docking and molecular dynamics simulations to evaluate active compounds of *Hibiscus schizopetalus* for obesity. *Journal of Applied Pharmaceutical Science*, *14*(4), 176–187. https://doi.org/10.7324/JAPS.2024.158550

Bae, J.-Y., Choi, J.-S., Choi, Y.-J., Shin, S.-Y., Kang, S.-W., Han, S. J., & Kang, Y.-H. (2008). (−)Epigallocatechin gallate hampers collagen destruction and collagenase activation in ultraviolet-B-irradiated human dermal fibroblasts: Involvement of mitogen-activated protein kinase. *Food and Chemical Toxicology*, *46*(4), 1298–1307. https://doi.org/10.1016/j.fct.2007.09.112

Bell, E. W., & Zhang, Y. (2019). DockRMSD: An open-source tool for atom mapping and RMSD calculation of symmetric molecules through graph isomorphism. *Journal of Cheminformatics*, *11*(1), 40. https://doi.org/10.1186/s13321-019-0362-7

Carbone, K., Gervasi, F., Kozhamzharova, L., Altybaeva, N., Sönmez Gürer, E., Sharifi-Rad, J., Hano, C., & Calina, D. (2023). Casticin as potential anticancer agent: Recent advancements in multi-mechanistic approaches. *Frontiers in Molecular Biosciences*, *10*, 1157558. https://doi.org/10.3389/fmolb.2023.1157558

Chakrabarti, B., Bairagya, H. R., Mukhopadhyay, B. P., & Sekar, K. (2017). New biochemical insight of conserved water molecules at catalytic and structural Zn2+ ions in human matrix metalloproteinase-I: A study by MD-simulation. *Journal of Molecular Modeling*, *23*(2), 57. https://doi.org/10.1007/s00894-017-3210-6

Cui, B., Wang, Y., Jin, J., Yang, Z., Guo, R., Li, X., Yang, L., & Li, Z. (2022). Resveratrol treats UVB-induced photoaging by anti-MMP expression, through anti-inflammatory, antioxidant, and antiapoptotic properties, and treats photoaging by upregulating VEGF-B expression. *Oxidative Medicine and Cellular Longevity*, *2022*, 6037303. https://doi.org/10.1155/2022/6037303

Demeule, M., Brossard, M., Pagé, M., Gingras, D., & Béliveau, R. (2000). Matrix metalloproteinase inhibition by green tea catechins. *Biochimica et Biophysica Acta*, *1478*(1), 51–60. https://doi.org/10.1016/S0167-4838(00)00009-1

Dorjay Tamang, J. S., Banerjee, S., Baidya, S. K., Das, S., Ghosh, B., Jha, T., & Adhikari, N. (2025). An overview of matrix metalloproteinase-12 in multiple disease conditions, potential selective inhibitors, and drug designing strategies. *European Journal of Medicinal Chemistry*, *283*, 117154. https://doi.org/10.1016/j.ejmech.2024.117154

Feng, C., Chen, X., Yin, X., Jiang, Y., & Zhao, C. (2024). Matrix metalloproteinases on skin photoaging. *Journal of Cosmetic Dermatology*, *23*(12), 3847–3862. https://doi.org/10.1111/jocd.16558

Gimeno, A., Beltrán-Debón, R., Mulero, M., Pujadas, G., & Garcia-Vallvé, S. (2020). Understanding the variability of the S1′ pocket to improve matrix metalloproteinase inhibitor selectivity profiles. *Drug Discovery Today*, *25*(1), 38–57. https://doi.org/10.1016/j.drudis.2019.07.013

Irsal, R. A. P., Gholam, G. M., Dwicesaria, M. A., & Chairunisa, F. (2024). Computational investigation of *Y. aloifolia* variegate as anti-human immunodeficiency virus (HIV) targeting HIV-1 protease: A multiscale in-silico exploration. *Pharmacological Research – Modern Chinese Medicine*, *11*, 100451. https://doi.org/10.1016/j.prmcm.2024.100451

Islam, M. T., Jang, N. H., & Lee, H. J. (2024). Natural products as regulators against matrix metalloproteinases for the treatment of cancer. *Biomedicines*, *12*(4), 794. https://doi.org/10.3390/biomedicines12040794

Land, H., & Humble, M. S. (2018). YASARA: A tool to obtain structural guidance in biocatalytic investigations. In *Methods in molecular biology* (pp. 43–67). Humana Press. https://doi.org/10.1007/978-1-4939-7366-8_4

Maghfira, H., Harnelly, E., Utomo, D. H., & Zulkarnain. (2025). Molecular modelling studies of anti-photoaging activity of patchouli (*Pogostemon cablin* Benth.) essential oil. *Tropical Journal of Natural Product Research*, *9*(1). https://doi.org/10.26538/tjnpr/v9i1.48

Mahayasih, P. G. M. W., Hartrianti, P., Parikesit, A. A., Clarisa, C., Widodo, F. K. T., Lestari, N. D., Wirawan, M. L., Fadhila, R., Chriscensia, E., Mun'im, A., James, R. J., Mubarok, S., Yan, C. C., & Ariestanti, D. M. (2026). Targeting skin aging at multiple fronts: Integrated in silico and in vitro evidence of antioxidant, anti-protease, and UVB-protective effects of *Vitex trifolia*. *International Journal of Molecular Sciences*, *27*(4), 1913. https://doi.org/10.3390/ijms27041913

Masruri, M., Safitri, A., Ulfa, S. M., Ferdian, R. F., Fabri, A. R. A., Karta, I. W., Harrist, M., & Shalsadila, A. A. (2025). Phytochemical composition, antioxidant activity, and metabolite profiling of sequential extracts from *Vitex trifolia* leaves with antibacterial potential: An integrated in vitro and in silico study. *Tropical Journal of Natural Product Research*, *9*(7), 2981–2992. https://doi.org/10.26538/tjnpr/v9i7.5

Mathpal, S., Sharma, P., Joshi, T., Pande, V., Mahmud, S., Jeong, M. K., Obaidullah, A. J., Chandra, S., & Kim, B. (2022). Identification of zinc-binding inhibitors of matrix metalloproteinase-9 to prevent cancer through deep learning and molecular dynamics simulation approach. *Frontiers in Molecular Biosciences*, *9*, 857430. https://doi.org/10.3389/fmolb.2022.857430

Mechqoq, H., Hourfane, S., El Yaagoubi, M., El Hamdaoui, A., da Silva Almeida, J. R. G., Rocha, J. M., & El Aouad, N. (2022). Molecular docking, tyrosinase, collagenase, and elastase inhibition activities of argan by-products. *Cosmetics*, *9*(1), 24. https://doi.org/10.3390/cosmetics9010024

Misra, M., & Yadav, A. K. (2022). Assessment of available AMBER force fields to model DNA–ligand interactions. *Biointerface Research in Applied Chemistry*, *13*(2), 156. https://doi.org/10.33263/BRIAC132.156

Nutho, B., & Tungmunnithum, D. (2023). Exploring major flavonoid phytochemicals from *Nelumbo nucifera* Gaertn. as potential skin anti-aging agents: In silico and in vitro evaluations. *International Journal of Molecular Sciences*, *24*(23), 16571. https://doi.org/10.3390/ijms242316571

Păcularu-Burada, B., Cîrîc, A. I., & Begea, M. (2024). Anti-aging effects of flavonoids from plant extracts. *Foods*, *13*(15), 2441. https://doi.org/10.3390/foods13152441

Ramchandani, S., Naz, I., Lee, J. H., Khan, M. R., & Ahn, K. S. (2020). An overview of the potential antineoplastic effects of casticin. *Molecules*, *25*(6), 1287. https://doi.org/10.3390/molecules25061287

Tan, L. H., Kwoh, C. K., & Mu, Y. (2024). RmsdXNA: RMSD prediction of nucleic acid–ligand docking poses using machine-learning method. *Briefings in Bioinformatics*, *25*(3), bbae166. https://doi.org/10.1093/bib/bbae166

Wu, N., Zhang, R., Peng, X., Fang, L., Chen, K., & Jestilä, J. S. (2024). Elucidation of protein–ligand interactions by multiple trajectory analysis methods. *Physical Chemistry Chemical*

Physics, *26*(8), 6903–6915. https://doi.org/10.1039/D3CP03492E

Zhang, M., Xue, Y., Chen, H., Meng, L., Chen, B., Gong, H., Zhao, Y., & Qi, R. (2019). Resveratrol inhibits MMP3 and MMP9 expression and secretion by suppressing TLR4/NF-κB/STAT3 activation in Ox-LDL-treated HUVECs. *Oxidative Medicine and Cellular Longevity*, *2019*, 9013169. https://doi.org/10.1155/2019/9013169

Zheng, D., Jiang, S., Zheng, P., Zhou, D., Qiu, J., & Gao, L. (2024). Molecular mechanism for the interaction of natural products with ionic liquids: Insights from MD and DFT study. *Journal of Molecular Liquids*, *399*, 124440. https://doi.org/10.1016/j.molliq.2024.124440

Publisher's Note & Disclaimer

All statements, opinions, and data in this publication were solely the responsibility of the individual authors or contributors and did not necessarily reflect the views of the publisher or editors. The publisher and editors did not guarantee the accuracy, completeness, or reliability of the content, and were not legally responsible for any errors, omissions, or consequences arising from its use. The publisher and editors also disclaimed any liability for injury, damage, or loss to persons or property resulting from the application of ideas, methods, or products mentioned herein. Readers were advised to independently verify all information before relying on it. The publisher accepted no responsibility for any consequences arising from the use of this publication's materials.